Journal of Information Systems Engineering and Management
2026, 11(3s)
e-ISSN: 2468-4376
https://www.jisem-journal.com/

Research Article

Direct Power Control of a Three-Phase PWM Rectifier Based on Backstepping with Integral Action for Enhanced Robustness and Power Quality

Ali El habib Ameur [1], Tarik Mohammed Chikouche[2], Kada Hartani[3]
[1,2,3] Electrotechnical Engineering Laboratory, University of Saida Dr Tahar Moulay Saida, Algeria

ARTICLE INFO

Received: 26 Dec 2024

Revised: 14 Feb 2025

Accepted: 22 Feb 2025

ABSTRACT

Introduction: Three-phase pulse-width modulation (PWM) rectifiers require highly efficient control strategies to ensure power quality and system stability. While Direct Power Control (DPC) is widely used, standard approaches often struggle with steady-state errors, power ripples, and sensitivity to load variations.

Objectives: This paper aims to design and validate an advanced DPC strategy that enhances tracking accuracy, eliminates steady-state errors, and improves the overall robustness of a three-phase PWM rectifier under diverse operating conditions.

Methods: The proposed control strategy integrates a nonlinear backstepping design with an added integral action. This combination is specifically engineered to handle system nonlinearities while actively compensating for load variations. The performance and validation of the control loop were carried out through comprehensive simulations within the MATLAB/Simulink environment.

Results: The simulation results demonstrate that the proposed strategy significantly minimizes active and reactive power ripples, reduces the Total Harmonic Distortion (THD) of the grid side currents, and consistently achieves a unity power factor. Furthermore, the system successfully eliminates steady-state errors under load variations.

Conclusions: The backstepping DPC with integral action proves to be a highly effective solution for three-phase PWM rectifiers. It delivers a fast dynamic response, robust disturbance rejection, and superior power quality, making it a viable option for high-performance power conversion applications.

Keywords: Direct Power Control (DPC), Backstepping control, Three-phase PWM rectifier, Integral action, Power quality.

1. INTRODUCTION

Power electronics converters play an important role in industrial applications and electrical networks. In industrial applications, they are used to vary the speed of electric machines and to charge batteries of electric vehicles, etc. In electrical networks, they are used for transmitting energy in the form of high-voltage direct current, for regulating the speed of generators, particularly in wind energy production systems, as well as for optimizing the energy production of wind and photovoltaic systems. Many other applications of these converters are not mentioned here.

A rectifier is a type of power electronic converter that enables the conversion of alternating current (AC) into direct current (DC). It is commonly represented as an AC/DC converter in electrical schematics. Rectifiers are generally classified into two main categories: uncontrolled rectifiers and controlled rectifiers. In both cases, they may be implemented as single-phase or three-phase systems depending on the application requirements. Uncontrolled rectifiers, typically based on diodes, offer the advantages of simplicity, high reliability, and low cost. However, they

Journal of Information Systems Engineering and Management
2026, 11(3s)
e-ISSN: 2468-4376
https://www.jisem-journal.com/
Research Article

suffer from several limitations, including unidirectional power flow, poor input power factor, and the generation of highly distorted input currents with significant harmonic content.

In contrast, controlled rectifiers, particularly pulse-width modulation (PWM) rectifiers, provide a more advanced and flexible solution for industrial applications. They allow bidirectional power flow, enable regulation of the input power factor, and ensure precise control of the DC bus voltage. Nevertheless, the overall performance of PWM rectifiers, especially in terms of current harmonic distortion, strongly depends on the adopted control strategy [1–3]. The main objective of modern control approaches is to achieve a near-unity power factor and to obtain quasi-sinusoidal input currents with minimal harmonic distortion [4]. To this end, numerous control strategies have been proposed in the literature [5]. Among them, two main approaches are widely used for PWM rectifier control: Voltage Oriented Control (VOC) and Direct Power Control (DPC).

The Voltage Oriented Control (VOC) is one of the most widely used methods for PWM rectifier power control. It is based on current regulation using proportional–integral (PI) controllers or hysteresis regulators [6][7]. However, its performance is sensitive to parameter variations and grid disturbances, such as unbalanced supply conditions. Moreover, due to the nonlinear nature of PWM converter models, linear controllers may lead to suboptimal dynamic behavior. Nonlinear approaches, such as sliding-mode control, have been introduced to improve robustness. However, they may generate undesirable chattering and interference effects, particularly at low switching frequencies [8][9]. In this context, Direct Power Control (DPC) offers a simpler structure and faster dynamic response. It directly regulates active and reactive powers using a predefined switching table for voltage vector selection, achieving higher accuracy than VOC [10]. Nevertheless, conventional DPC suffers from significant steady-state power ripple and variable switching frequency [11]. To overcome these limitations, several improved switching strategies have been proposed to reduce ripple and enhance dynamic performance [12][13]. Further developments include predictive control techniques based on Space Vector Modulation (SVM) [3][14], which eliminate the switching table used in classical DPC. In Model Predictive Direct Power Control (MP-DPC), a mathematical model is used to predict future active and reactive power values. The control strategy selects multiple voltage vectors within a single sampling period, where the optimization of active power ripple determines the optimal vector durations [15–18].

The backstepping control (BSC) methodology has received significant attention due to its systematic recursive design for nonlinear control systems [19–21]. It relies on virtual control inputs for lower-order subsystems and ensures stability through a Lyapunov-based construction of a global function. This approach has been widely applied in renewable energy systems such as wind and solar energy conversion [22][23]. A BSC-DPC strategy for grid-connected AC/DC converters has shown good dynamic performance under grid imbalance conditions. However, its robustness is limited due to neglected parameter uncertainties and external disturbances [21][24].

Classical backstepping may also suffer from performance degradation under sudden load changes or model inaccuracies. The tracking error typically converges to a bounded residual set depending on disturbance levels [25][26], which is critical in applications like hybrid electric vehicles (HEVs) with varying load conditions. To improve robustness, Integral Backstepping Control (IBSC) introduces an integral state into the system dynamics, eliminating steady-state errors and improving disturbance rejection. Two main implementations exist: integral augmentation and Lyapunov redesign [25][26]. The system is reformulated in strict-feedback form and then processed using standard backstepping on the augmented model [29][30]. Applications such as induction motor control (IFOC) show that IBSC significantly reduces speed tracking errors under sudden load torque variations [28][29]. The integral action effectively compensates disturbances and enhances overall robustness.

This study is an extended and improved version of a three-phase rectifier controlled by a backstepping-based BSC-DPC system. An integral action is introduced to further enhance the overall performance. This work is organized into four sections to better address the objectives of the research. Section 2 presents the modeling of the two-level PWM rectifier power circuit. Section 3 is entirely dedicated to the integral backstepping direct power control of the PWM rectifier. An appropriate mathematical model of active and reactive power is developed and analyzed to achieve reduced power ripple and quasi-sinusoidal input currents. Section 4 presents the simulation results and discussion, followed by the conclusion.

Journal of Information Systems Engineering and Management
2026, 11(3s)
e-ISSN: 2468-4376
https://www.jisem-journal.com/
Research Article

2. MODEL OF THREE-PHASE PWM RECTIFIER

The objective of modeling is to establish a relationship between control variables and electrical quantities. To model the PWM rectifier, three main stages must be considered: the source, the converter, and the load, while also taking into account the output voltage control and switching control parts. The circuit structure of a three-phase PWM rectifier is shown in Fig. 1.

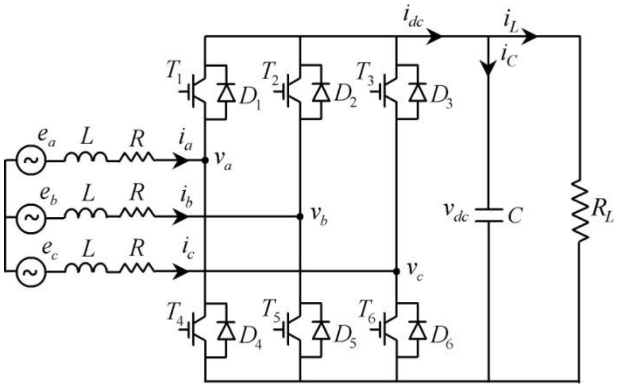

Figure 1. Circuit structure of three-phase PWM rectifier.

To develop the mathematical model, it is assumed that the AC voltage is a balanced three-phase supply, the filter reactor is linear, and the IGBT is an ideal and lossless switch. Generally, a three-phase rectifier is modeled in a stationary abc system(a, b, c), however, to facilitate the determination of the control law, it is necessary to transform this system into a two-phase system. According to the three-phase-to-two-phase transformation and by applying Kirchhoff's voltage law, the mathematical model of a PWM rectifier in a stationary (α−β) reference frame is obtained as follows [3]:

$$\begin{cases} L\frac{di_\alpha}{dt} = e_\alpha - R.i_\alpha - v_\alpha \\ L\frac{di_\beta}{dt} = e_\beta - R.i_\beta - v_\beta \\ L\frac{di_\beta}{dt} = i_{dc} - i_L \end{cases} \quad (1)$$

Where, e_α, e_β are the source-voltage vector in the(α, β) reference frame, v_α, v_β are the rectifier-voltage vector in the(α, β) referenceframe,i_α, i_β are currents vector in the (α, β) reference frame and R, L are mean resistance and inductance of the filter reactor respectively,

The instantaneous active power and the reactive power (P, Q) in the (α, β) reference frame can be expressed as follows [30][31]:

$$\begin{cases} P = e_\alpha i_\alpha + e_\beta i_\beta \\ Q = e_\beta i_\alpha + e_\alpha i_\beta \end{cases} \quad (2)$$

3. PROPOSED OF IBSC- DPC

At the beginning of each switching period, the rectifier phase voltages and line currents are measured and transformed into the stationary (α−β) reference frame. To generate the active power reference, the measured output DC-link voltage is compared with its predefined reference value, and the resulting error is processed through an Integral-Proportional (IP) controller [12, 24].

The active and reactive powers are regulated using backstepping control, a nonlinear technique derived from Lyapunov stability theory. This control principle is based on decomposing the global system into a series of cascaded subsystems. At each design stage, a "virtual control law" is synthesized to stabilize the respective subsystem, while a control Lyapunov function (CLF) is constructed to guarantee the asymptotic stability of the tracking error between the actual state and the virtual command.

Journal of Information Systems Engineering and Management
2026, 11(3s)
e-ISSN: 2468-4376
https://www.jisem-journal.com/

Research Article

To enhance robustness, Integral Backstepping Control (IBSC) is introduced as a variant of the conventional backstepping approach. By incorporating an integral action into the error variables—defined as the mismatch between the actual and desired system states—the IBSC framework effectively eliminates steady-state errors and rejects external disturbances. Consequently, the IBSC-DPC scheme computes the required control voltages (vα and vβ), which are subsequently supplied to the Space Vector Modulation (SVM) block to generate the switching signals for the rectifier's power switches (IGBTs) [21]. The overall architecture of the proposed IBSC-DPC technique for the PWM rectifier is illustrated in Figure 2.

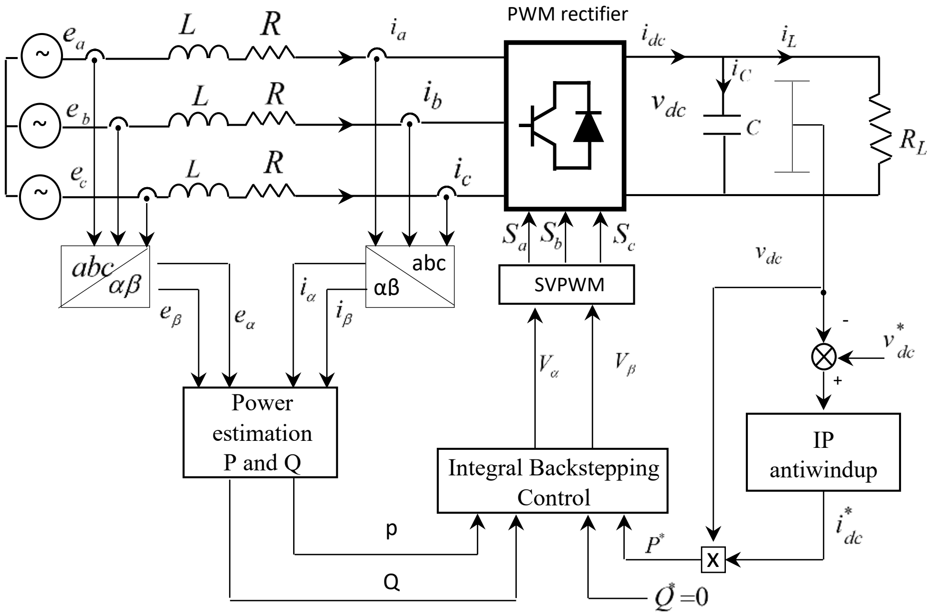

Figure 2. Proposed IBSC-DPC configuration of three-phase PWM rectifier.

This theory has been widely described in [33]-[36]. The integral backstepping approach is described by the following three main step :

1. Tracking error identification;
2. Selection of the Lyapunov function to ensure system stability;
3. Determination of the equivalent control current laws.

Step 1: The primary objective of using integral backstepping is to ensure that the measured value accurately tracks the reference trajectory. Consequently, the active power tracking error is defined as follows:

$$\begin{cases} Z_P = P - P^* + k'_p \int_0^t (P - P^*).dt \\ Z_Q = Q - Q^* + k'_Q \int_0^t (Q - Q^*).dt \end{cases} \tag{3}$$

Where$k'_p \int_0^t (P - P^*).dt$, $k'_p \int_0^t (Q - Q^*).dt$ and are an integral action added to the active and reactive power respectively, and k'_p, k'_Q are a positive design constant.

The derivative of the P and Q is :

$$\begin{cases} \dot{P} = \dot{e_\alpha} i_\alpha + \frac{e_\alpha e_\alpha}{L} - R.\frac{e_\alpha}{L} i_\alpha - \frac{e_\alpha}{L} v_\alpha + \dot{e_\beta} i_\beta + \frac{e_\beta e_\beta}{L} - R.\frac{e_\beta}{L} i_\beta - \frac{e_\beta}{L} v_\beta \\ \dot{Q} = \dot{e_\alpha} i_\alpha + \frac{e_\beta e_\alpha}{L} - R.\frac{e_\beta}{L} i_\alpha - \frac{e_\beta}{L} v_\alpha - \dot{e_\alpha} i_\beta - \frac{e_\alpha e_\beta}{L} + R.\frac{e_\alpha}{L} i_\beta + \frac{e_\alpha}{L} v_\beta \end{cases} \tag{4}$$

This error derivative is:

$$\begin{cases} \dot{Z_P} = \dot{P} - \dot{P^*} + k'_p(\dot{P} - \dot{P^*}) \\ \dot{Z_Q} = \dot{Q} - \dot{Q^*} + k'_Q(\dot{Q} - \dot{Q^*}) \end{cases} \tag{5}$$

Journal of Information Systems Engineering and Management
2026, 11(3s)
e-ISSN: 2468-4376
https://www.jisem-journal.com/
Research Article

By replacing the equation (3) in equation (5) , leads to :

$$\begin{cases} \dot{Z}_P = \left(\dot{e_\alpha} i_\alpha + \frac{e_\alpha e_\alpha}{L} - R.\frac{e_\alpha}{L} i_\alpha - \frac{e_\alpha}{L} v_\alpha + \dot{e_\beta} i_\beta + \frac{e_\beta e_\beta}{L} - R.\frac{e_\beta}{L} i_\beta - \frac{e_\beta}{L} v_\beta\right) - \dot{P}^* + k_p'(\dot{P} - \dot{P}^*) \\ \dot{Z}_Q = \left(\dot{e_\alpha} i_\alpha + \frac{e_\beta e_\alpha}{L} - R.\frac{e_\beta}{L} i_\alpha - \frac{e_\beta}{L} v_\alpha - \dot{e_\alpha} i_\beta - \frac{e_\alpha e_\beta}{L} + R.\frac{e_\alpha}{L} i_\beta + \frac{e_\alpha}{L} v_\beta\right) - \dot{Q}^* + k_Q'(\dot{Q} - \dot{Q}^*) \end{cases} \tag{6}$$

Step 2: The stability of the closed-loop system is established using Lyapunov's stability theorem. To ensure that the active and reactive power tracking errors converge to zero, the initial candidate Lyapunov function is defined as follows:

$$\begin{cases} V_P = \frac{1}{2} Z_P^2 \\ V_Q = \frac{1}{2} Z_Q^2 \end{cases} \tag{7}$$

The active and reactive power tracking errors are stable and converge to zero when the Lyapunov function is positive-definite and its time derivative is negative-definite, as discussed in [34]–[37]. Here, k represents a positive constant. Since the time derivative of the Lyapunov function is negative-definite, the system is asymptotically stable.

$$\begin{cases} \dot{V}_P = Z_P \dot{Z}_P = -kZ_P^2 < 0 \\ \dot{V}_Q = Z_Q \dot{Z}_Q = -kZ_Q^2 < 0 \end{cases} \tag{8}$$

From (7) and (8): the derivative of the Lyapunov function is obtained, as follows :

$$\begin{cases} Z_P\left[\dot{e_\alpha} i_\alpha + \frac{e_\alpha e_\alpha}{L} - R.\frac{e_\alpha}{L} i_\alpha - \frac{e_\alpha}{L} v_\alpha + \dot{e_\beta} i_\beta + \frac{e_\beta e_\beta}{L} - R.\frac{e_\beta}{L} i_\beta - \frac{e_\beta}{L} v_\beta - \dot{P}^* + k_p'\left(\dot{P} - \dot{P}^*\right)\right] = -kZ_P^2 \\ Z_Q\left[\dot{e_\alpha} i_\alpha + \frac{e_\beta e_\alpha}{L} - R.\frac{e_\beta}{L} i_\alpha - \frac{e_\beta}{L} v_\alpha - \dot{e_\alpha} i_\beta - \frac{e_\alpha e_\beta}{L} + R.\frac{e_\alpha}{L} i_\beta + \frac{e_\alpha}{L} v_\beta - \dot{Q}^* + k_Q'(\dot{Q} - \dot{Q}^*)\right] = -kZ_P^2 \end{cases} \tag{9}$$

Step 3: Assuming that the v_α and v_β voltages remain equal to their respective reference values at all times, the control laws can be derived as follows:

$$\begin{cases} v_\alpha = \frac{L}{e_\alpha} \dot{e_\alpha} i_\alpha + e_\alpha - R.i_\alpha + \frac{L}{e_\alpha} \dot{e_\beta} i_\beta + \frac{e_\beta e_\beta}{e_\alpha} - R.\frac{e_\beta}{e_\alpha} i_\beta - \frac{e_\beta}{e_\alpha} v_\beta v_\beta - \frac{L}{e_\alpha} \dot{P}^* + \frac{L}{e_\alpha} k_p'\left(\dot{P} - \dot{P}^*\right) + \frac{L}{e_\alpha} kZ_P^2 \\ v_\beta = -\frac{L}{e_\alpha} \dot{e_\alpha} i_\alpha + R.\frac{e_\beta}{e_\alpha} i_\alpha + \frac{e_\beta}{e_\alpha} v_\alpha + \frac{L}{e_\alpha} \dot{e_\alpha} i_\beta - R.i_\beta + \frac{L}{e_\alpha} \dot{Q}^* - \frac{L}{e_\alpha} k_Q'\left(\dot{Q} - \dot{Q}^*\right) - \frac{L}{e_\alpha} kZ_P^2 \end{cases} \tag{10}$$

3.2. SVPWM method

Compared to conventional approaches—such as hysteresis control of the rectifier legs to track sinusoidal references or specific PWM techniques for harmonic elimination—Space Vector Pulse Width Modulation (SVPWM) has emerged as a superior control method to enhance rectifier performance. According to [3], [37], the primary objectives of an SVPWM-controlled rectifier are to:

- Maintain a constant and adjustable DC-link voltage, regardless of load variations and grid disturbances;
- Ensure a unitary power factor (UPF) at the Point of Common Coupling (PCC);
- Enable bidirectional power flow for energy regeneration;
- Minimize line-side current harmonics injected into the grid by the rectifier switching actions.

The Space Vector Pulse Width Modulation (SVPWM) technique determines the voltage vectors to be applied and their corresponding application times analytically through mathematical equations. Each possible switching state of the converter is represented by a voltage vector, and all these vectors collectively form the converter voltage vector diagram. Unlike conventional PWM techniques, SVPWM generates the control signals by simultaneously considering the switching states of all three converter legs.

Depending on the switching state shown in Figure 1, the converter can assume eight distinct switching states, which are represented by eight voltage vectors (V0 to V7) in the $\alpha - \beta$ reference frame. These vectors are illustrated in Figure 4. Among them, six are active (non-zero) voltage vectors (V1 to V6), while two are zero voltage vectors (V0 and V7). The active vectors have identical magnitudes, equal to (2/3)Vdc, where Vdc is the DC-link voltage. The

Journal of Information Systems Engineering and Management
2026, 11(3s)
e-ISSN: 2468-4376
https://www.jisem-journal.com/
Research Article

three-phase output voltage can therefore be represented by a single rotating voltage vector in the $\alpha - \beta$ plane, which constitutes the fundamental principle of SVPWM.

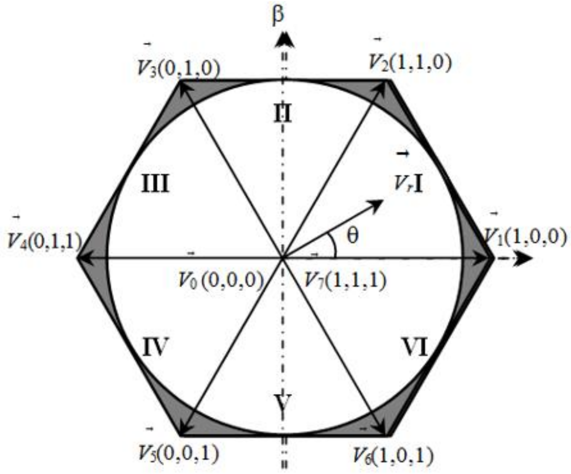

Figure 4. Space voltage vectors.

4. SIMULATION AND RESULT DISCUSSION

To confirm the effectiveness of the proposed IBSC-DPC, a simulation test was carried out on a two-level three-phase PWM rectifier using MATLAB/Simulink. The main parameters of the simulation circuit are summarized in Table 2.

Table 2. Rectifier parameters.

The input phase voltage :	V=125 V / f=50Hz
The input inductance :	L= 37 mH
The input resistance :	R= 0.3 Ω
The output capacitor :	C= 1100 µF
The output voltage :	vdc = 350 V

The simulation results were obtained using MATLAB/Simulink for a three-phase PWM rectifier controlled by the IBCS-DPC strategy with DC bus voltage regulation. Accordingly, the corresponding results are presented in Fig. 5.

Fig. 5(a) illustrates the dynamic performance of the DC-link voltage under the proposed control strategy. At startup (t = 0s), the actual voltage rapidly reaches its initial reference of 350V in less than 0.05s. When a step change from 350V to 450V is applied at t = 0.25s, the controller ensures fast and accurate tracking with a settling time of approximately 0.08s and no visible overshoot. Furthermore, the sudden load disturbance introduced between t = 0.5s and t = 0.7s has a negligible impact, as the voltage remains firmly stable at 450V. Fig. 5(b) provides a detailed zoom-in view of the DC-link voltage (Vdc) response during the load disturbance interval (t=0.4 s to 0.9 s). A closer inspection reveals that when the sudden load disturbance is applied at t=0.5 s, the actual voltage experiences a minor and brief voltage drop (undershoot) of merely 1 V, dropping from 450 V to 449 V. Thanks to the fast corrective action of the proposed controller, the voltage recovers swiftly and returns to its reference value of 450 V in less than 0.05 s (t≈0.55 s). Conversely, when the load disturbance is removed at t=0.7 s, a very slight voltage overshoot of about 0.8 V is observed, which is also rapidly eliminated within 0.04 s. These zoom-in results clearly demonstrate that the voltage fluctuations remain restricted within an extremely narrow margin (less than 0.25%), confirming the exceptional disturbance rejection capability, high dynamic stiffness, and superior robustness of the developed control strategy against sudden load variations. These results successfully demonstrate the high tracking

Journal of Information Systems Engineering and Management
2026, 11(3s)
e-ISSN: 2468-4376
https://www.jisem-journal.com/
Research Article

capability, fast dynamic response, and strong robustness of the developed regulator against external perturbations in both transient and steady-state regimes.

Fig. 5(c) illustrates the profile of the load disturbance applied to the system to evaluate its robustness. Initially, the rectifier operates under a steady-state load resistance of 500 Ω. At t=0.5 s, a sudden step change is introduced, causing the load resistance to drop abruptly by half, from 500 Ω to 250 Ω, which significantly increases the power demand on the DC-link. This severe load condition is maintained for a duration of 0.2 s. Subsequently, at t=0.7 s, the load resistance steps back up to its initial value of 500 Ω.

The dynamic behavior and performance of the three-phase grid currents (ia,ib,ic) under the proposed IBSC-DPC strategy are illustrated in Fig. 5(d), with detailed close-ups during the load transitions presented in Fig. 5(e) and Fig. 5(f). Throughout the entire simulation, the grid currents maintain a highly balanced, symmetric, and quasi-sinusoidal waveform. At t=0.25 s, a brief transient overshoot in the current amplitude occurs, which corresponds to the sudden energy required to charge the DC-link capacitor to its new reference (450 V). As zoomed-in in Fig. 5(e), when the load resistance drops from 500 Ω to 250 Ω at t=0.5 s, the current amplitude instantaneously and smoothly doubles from 1 A to 2 A to satisfy the higher active power demand without any phase displacement or distortion. Conversely, Fig. 5(f) shows that when the load disturbance is removed at t=0.7 s, the current amplitude immediately drops back to 1 A within less than half a cycle. These results clearly demonstrate the high dynamic reactivity, seamless transition capabilities, and excellent power quality preserved by the developed controller under severe load variations.

The time-domain behavior of the grid currents in the α-β stationary frame (iα and iβ) exhibits three distinct phases, Fig. 5(g). Following an initial transient period characterized by large oscillations between 0 and 0.05 s, the currents rapidly stabilize at a near-zero amplitude. At t = 0.5s, the application of a disturbance (or load step) induces a clear increase in amplitude, reaching approximately 3 A. The close-up views reveal perfectly sinusoidal waveforms in quadrature, confirming the proper operation of the control system in the stationary frame. Finally, at t = 0.7s, the currents return to their initial low-amplitude state, demonstrating the system's robustness and fast dynamic response to load variations.

The figure 5(h) illustrates the grid phase voltage va and the corresponding phase current ia waveforms (scaled by a factor of 50). Both signals are perfectly sinusoidal and strictly in phase throughout the displayed time interval (0.48 s to 0.58 s). This tight phase alignment demonstrates that a unity power factor (UPF) is successfully achieved on the grid side. Furthermore, following the reference step change at t=0.5 s, the current amplitude seamlessly adjusts (from a scaled peak value of 50 A to 100 A, corresponding to an actual current step from 1 A to 2 A) while maintaining perfect synchronism with the voltage. This confirms the high effectiveness and fast dynamic tracking of the current control loop.

The figures 5(i) and (j) illustrate the transient and steady-state responses of the active (P) and reactive (Q) powers compared to their respective references. It can be observed that the actual active power tracks its reference value with high fidelity and zero steady-state error, demonstrating a fast dynamic response. At t=0.25 s, the power quickly stabilizes at 250 W after a brief transient peak, and the load step applied between t=0.5 s and t=0.7 s smoothly drives the power to 550 W without any overshoot or oscillation. Concurrently, the reactive power is strictly maintained at zero (Q=0 VAR) throughout the entire simulation, unaffected by the step changes in active power. This decoupled control capability and excellent tracking performance validate the robustness, accuracy, and overall effectiveness of the proposed control strategy.

Figures 5(k) and 5(l) illustrate the single-period time-domain waveform and the Fast Fourier Transform (FFT) harmonic analysis of the grid phase current ia, respectively. The time-domain plot confirms a highly sinusoidal waveform with a period of 0.02 s (corresponding to a fundamental frequency of 50 Hz) and a peak fundamental amplitude of 1.018 A. The spectral analysis reveals a Total Harmonic Distortion (THD) of merely 2.04%. This value complies comfortably with the strict 5% limit mandated by international power quality standards, such as IEEE 519. The close-up view of the harmonic spectrum indicates a minor presence of the 3rd harmonic order (around 2% of the fundamental), while higher-order harmonics remain negligible. These quantitative findings demonstrate the

Journal of Information Systems Engineering and Management
2026, 11(3s)
e-ISSN: 2468-4376
https://www.jisem-journal.com/

Research Article

superior quality of the power injected into the grid and validate the high-filtering performance achieved by the implemented control strategy.

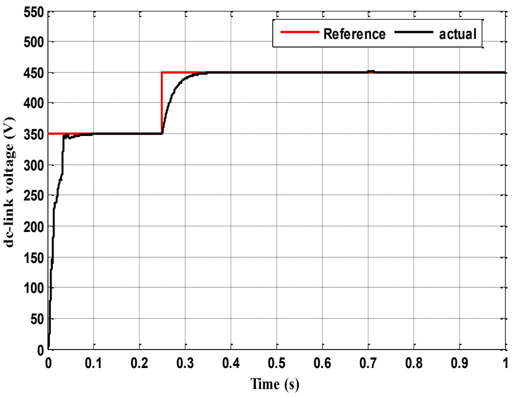

(a)

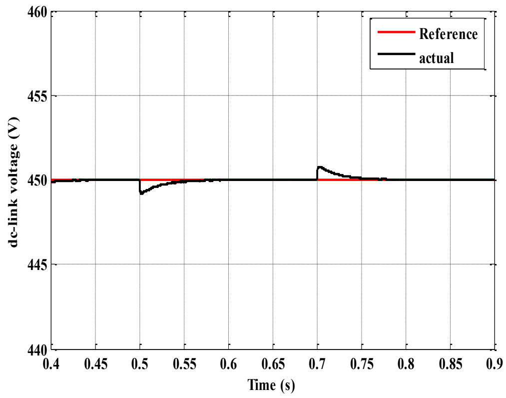

(b)

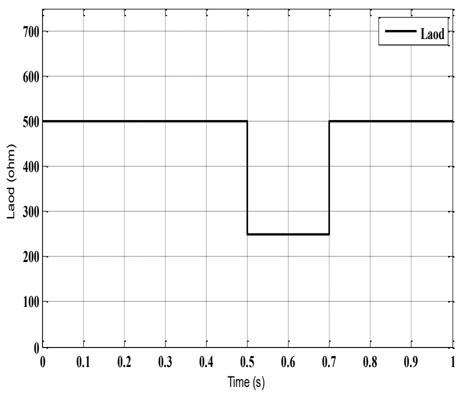

(c)

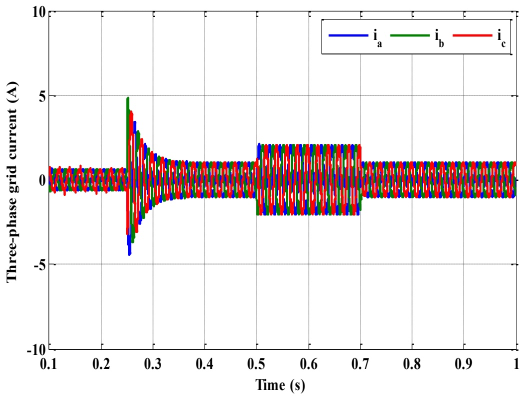

(d)

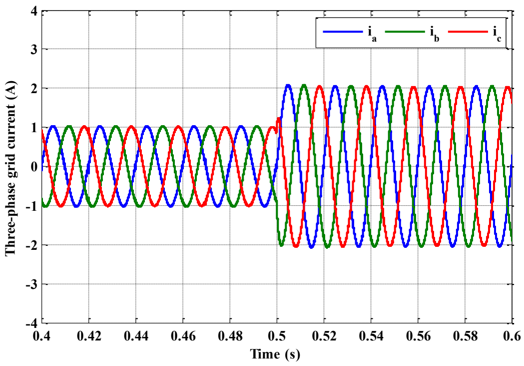

(e)

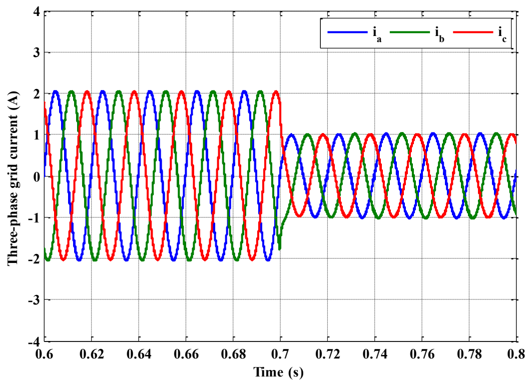

(f)

Journal of Information Systems Engineering and Management
2026, 11(3s)
e-ISSN: 2468-4376
https://www.jisem-journal.com/

Research Article

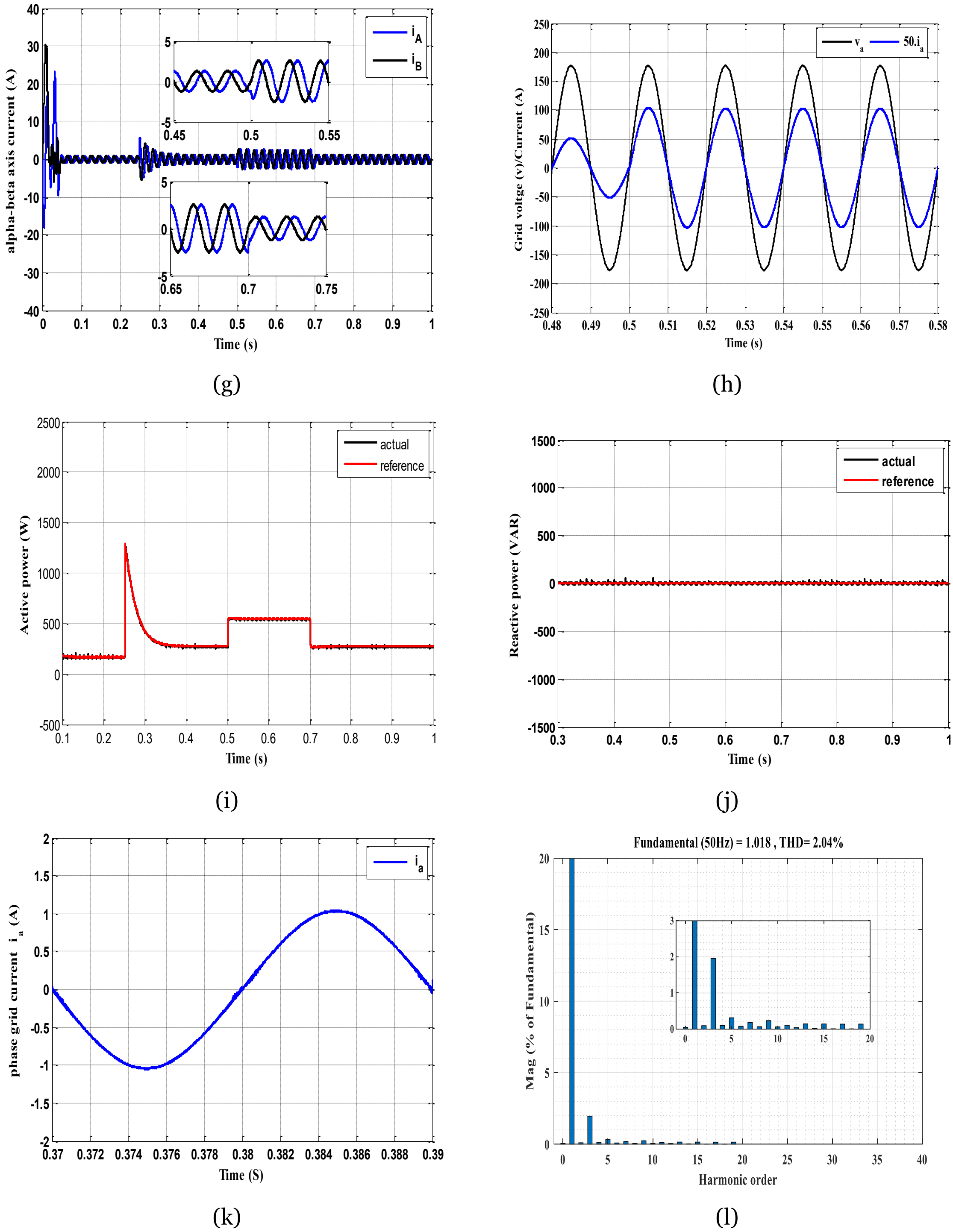

Figure 5 : Simulation results of proposed strategy

5. CONCLUSION

This paper has presented an Integral Backstepping Direct Power Control (IBSC-DPC) strategy for a three-phase PWM rectifier. The proposed controller ensures accurate DC-link voltage regulation while maintaining sinusoidal grid currents with a unity power factor. Simulation results demonstrate excellent tracking performance of the DC-link voltage and instantaneous active and reactive powers under various operating conditions. The grid currents remain balanced, sinusoidal, and synchronized with the supply voltages, ensuring high power quality. Compared with the conventional Backstepping approach, the proposed IBSC-DPC significantly reduces power ripples and improves both dynamic and steady-state performances. These results confirm the effectiveness, robustness, and reliability of the proposed control strategy for high-performance AC/DC power conversion applications.

REFRENCES

[1] Zhang, X., & Zhang, X. (2003). PWM rectifier and its control. *Bei Jing: China Machine Press˛2003*.
[2] Mallik, A., Ding, W., Shi, C., & Khaligh, A. (2016). Input voltage sensorless duty compensation control for a three-phase boost PFC converter. *IEEE Transactions on Industry Applications*, *53*(2), 1527-1537,doi.org/10.1109/TIA.2016.2626247.
[3] Hartani, K., & Miloud, Y. (2010). Control strategy for three phase voltage source PWM rectifier based on the space vector modulation. *Advances in Electrical and Computer Engineering*, *10*(3), 61-65, doi.org/10.4316/aece.2010.03010
[4] Verdelho, P., & Soares, V. (1997, July). A unity power factor PWM voltage rectifier based on the instantaneous active and reactive current i/sub d/-i/sub q/method. In *ISIE'97 Proceeding of the IEEE International Symposium on Industrial Electronics* (Vol. 2, pp. 411-416). IEEE, doi.org/10.1109/ISIE.1997.648977.
[5] Malinowski, M., Kazmierkowski, M. P., & Trzynadlowski, A. (2003). Review and comparative study of control techniques for three-phase PWM rectifiers. *Mathematics and computers in simulation*, *63*(3-5), 349-361,doi.org/10.1016/S0378-4754(03)00081-8
[6] Huang, J., Zhang, A., Zhang, H., & Wang, J. (2011, November). A novel fuzzy-based and voltage-oriented direct power control strategy for rectifier. In *IECON 2011-37th Annual Conference of the IEEE Industrial Electronics Society* (pp. 1115-1119). IEEE, doi.org/10.1109/IECON.2011.6119464
[7] Blasko, V., & Kaura, V. (2002). A new mathematical model and control of a three-phase AC-DC voltage source converter. *IEEE transactions on Power Electronics*, *12*(1), 116-123, doi.org/10.1109/63.554176
[8] Zhang, Y., Peng, Y., & Yang, H. (2015). Performance improvement of two-vectors-based model predictive control of PWM rectifier. *IEEE Transactions on Power Electronics*, *31*(8), 6016-6030, doi.org/10.1109/TPEL.2015.2498306
[9] Zhang, Y., Qu, C., Li, Z., & Zhang, Y. (2013, October). Mechanism analysis and experimental study of table-based direct power control. In *2013 international conference on electrical machines and systems (ICEMS)* (pp. 2213-2218). IEEE, doi.org/10.1109/ICEMS.2013.6713192
[10] Ohnishi, T. (1991, October). Three phase PWM converter/inverter by means of instantaneous active and reactive power control. In *Proceedings IECON'91: 1991 International Conference on Industrial Electronics, Control and Instrumentation* (pp. 819-824). IEEE, doi.org/10.1109/IECON.1991.239183
[11] Noguchi, T., Tomiki, H., Kondo, S., & Takahashi, I. (2002). Direct power control of PWM converter without power-source voltage sensors. *IEEE transactions on industry applications*, *34*(3), 473-479,
[12] Chikouche, T. M., & Hartani, K. (2018). Direct power control of three-phase PWM rectifier based on new switching table. *Journal of Engineering Science and Technology*, *13*(6), 1751-1763.
[13] Chikouche, T. M., & Hartani, K. (2018). A strategy of direct power control for PWM rectifier reducing ripple in instantaneous power. *Int. J. Electr. and Computer Eng.*, *12*(2), 113-118, *doi.org/10.5281/ZENODO.1315785*.
[14] Bouafia, A., Gaubert, J. P., & Krim, F. (2009). Predictive direct power control of three-phase pulsewidth modulation (PWM) rectifier using space-vector modulation (SVM). *IEEE transactions on power electronics*, *25*(1), 228-236, doi.org/10.1109/TPEL.2009.2028731.
[15] Chikouche, T. M., Hartani, K., & Terras, T. (2022). Predictive-DPC Based on Duty Cycle Control of PWM Rectifier under Unbalanced Network. *Periodica Polytechnica Electrical Engineering and Computer Science*, *66*(2), 139-147, *doi.org/10.5281/ZENODO.1315785*.
[16] Hadji, K., Hartani, K., Chikouche, T. M., & Ameur, A. E. (2021, March). Predictive direct power control of a three-phase three-level NPC PWM rectifier based on space vector modulation. In *2021 12th International Symposium on Advanced Topics in Electrical Engineering (ATEE)* (pp. 1-9). IEEE. doi.org/10.1109/ATEE52255.2021.9425052.
[17] Zhang, Y., Peng, Y., & Qu, C. (2016). Model predictive control and direct power control for PWM rectifiers with active power ripple minimization. *IEEE Transactions on Industry Applications*, *52*(6), 4909-4918, doi.org/10.1109/TIA.2016.2596240.

[18] Chikouche, T. M., Hartani, K., & Mankour, M. (2023). Model Predictive Direct Power Control with Duty Cycle Control of PWM Rectifier. *Przegląd Elektrotechniczny*, *99*, dx.doi.org/10.15199/48.2023.07.04.
[19] Wai, R. J., Yao, J. X., & Lee, J. D. (2014). Backstepping fuzzy-neural-network control design for hybrid maglev transportation system. *IEEE Transactions on Neural networks and learning systems*, *26*(2), 302-317, doi.org/10.1109/TNNLS.2014.2314718.
[20] Dehkordi, N. M., Sadati, N., & Hamzeh, M. (2016). A robust backstepping high-order sliding mode control strategy for grid-connected DG units with harmonic/interharmonic current compensation capability. *IEEE Transactions on Sustainable Energy*, *8*(2), 561-572, doi.org/10.1109/TSTE.2016.2611383.
[21] Sun, D., Wang, X., & Fang, Y. (2016). Backstepping direct power control without phase-locked loop of AC/DC converter under both balanced and unbalanced grid conditions. *IET Power Electronics*, *9*(8), 1614-1624, doi.org/10.1049/iet-pel.2015.0653
[22] Pervej, M. F., Roy, T. K., Tumpa, F. K., & Sarkar, M. I. (2016, December). Nonlinear backstepping controller design for a three-phase grid-connected photovoltaic system using DPC approach. In *2016 9th International Conference on Electrical and Computer Engineering (ICECE)* (pp. 407-410). IEEE, doi.org/10.1109/ICECE.2016.7853943
[23] Atallah, M., Benmahdjoub, M. A., Salhi, I., Mezouar, A., Saidi, Y., & Gaillard, A. (2025). Efficient nonlinear integral backstepping control for doubly fed induction generators-based wind farm under unbalanced electrical grid voltage. *International Journal of Electrical Power & Energy Systems*, *172*, 111141. doi.org/10.1016/j.ijepes.2025.111141.
[24] Wai, R. J., & Yang, Y. (2019). Design of backstepping direct power control for three-phase PWM rectifier. *IEEE Transactions on Industry Applications*, *55*(3), 3160-3173, doi.org/10.1109/TIA.2019.2893832.
[25] Fateh, M., & Abdellatif, R. (2017). Comparative study of integral and classical backstepping controllers in IFOC of induction motor fed by voltage source inverter. *International Journal of Hydrogen Energy*, *42*(28), 17953-17964,,doi.org/10.1016/j.ijhydene.2017.04.292
[26] Skjetne, R., & Fossen, T. I. (2004, June). On integral control in backstepping: Analysis of different techniques. In *Proceedings of the 2004 American control conference* (Vol. 2, pp. 1899-1904). IEEE, doi.org/10.23919/ACC.2004.1386858.
[27] Siffat, S. A., Ahmad, I., Rahman, A. U., & Islam, Y. (2020). Robust integral backstepping control for unified model of hybrid electric vehicles. *IEEE Access*, *8*, 49038-49052, DOI: 10.1109/ACCESS.2020.2978258
[28] Poultney, A., Gong, P., & Ashrafiuon, H. (2019). Integral backstepping control for trajectory and yaw motion tracking of quadrotors. *Robotica*, *37*(2), 300-320, DOI: 10.1017/S0263574718001029
[29] Jasim, W. M., & Gu, D. (2020). Integral backstepping controller for uavs team formation. In *Automation and Control*. IntechOpen, DOI: 10.5772/intechopen.93731
[30] Babar, S. A., Rana, I. A., Arslan, M., & Zafar, M. W. (2019). Integral backstepping based automated control of blood glucose in diabetes mellitus type 1 patients. *IEEE Access*, *7*, 173286-173293, DOI: 10.1109/ACCESS.2019.2951010
[31] Noguchi, T., Tomiki, H., Kondo, S., & Takahashi, I. (2002). Direct power control of PWM converter without power-source voltage sensors. *IEEE transactions on industry applications*, *34*(3), 473-479, https://doi.org/10.1109/28.673716
[32] Dalessandro, L., Round, S. D., & Kolar, J. W. (2008). Center-point voltage balancing of hysteresis current controlled three-level PWM rectifiers. *IEEE Transactions on Power Electronics*, *23*(5), 2477-2488, doi.org/10.1109/TPEL.2008.2002060.
[33] Fang, Z., & Gao, W. (2011, July). Adaptive integral backstepping control of a micro-quadrotor. In *2011 2nd International conference on intelligent control and information processing* (Vol. 2, pp. 910-915). IEEE, doi.org/10.1109/ICICIP.2011.6008382.
[34] M. Atallah, A. Mezouar, K. Belgacem, M.A. Benmahdjoub, Y. Saidi, B. Brahmi Grid synchronization of equivalent wind farm equipped with DFIG model for transient stability by using nonlinear integral backstepping control Arab J Sci Eng, 48 (2023), pp. 5771-5783, doi.org/10.1007/s13369-022-07021-y.
[35] Hamida, M. A., Ezzat, M., Glumineau, A., De Leon, J., & Boisliveau, R. (2012, July). Commande par Backstepping avec action intégrale pour la MSAP: Tests expérimentaux. In *Conférence Internationale Francophone d'Automatique (CIFA2012), Grenoble, France* (pp. 4-6).

[36] Wang, F., Chen, W., Dai, H., Li, J., & Jia, J. (2019). Backstepping control of a quadrotor unmanned aerial vehicle based on multi-rate sampling. *Science China. Information Sciences*, *62*(1), 19203, doi.org/10.1007/s11432-018-9542-3.

[37] Zhao, D., & Ayyanar, R. (2006, July). Space vector PWM with DC link voltage control and using sequences with active state division. In *2006 IEEE International Symposium on Industrial Electronics* (Vol. 2, pp. 1223-1228). IEEE, **DOI:** 10.1109/ISIE.2006.295812